JOURNAL OF CATALYSIS 134, 134–150 (1992)

Steady-State and Transient Kinetic Studies of Ethane Hydrogenolysis over Ru/Al_2O_3

S. B. SHANG AND C. N. KENNEY

Department of Chemical Engineering, University of Cambridge, Pembroke Street, Cambridge CB2 3RA, United Kingdom

Received April 18, 1991; revised August 14, 1991

Kinetic studies of ethane hydrogenolysis over supported ruthenium catalysts have been carried out under both steady-state and transient conditions. A wide range of steady-state models has been examined. Although great discrimination among the models cannot be obtained, the modified model proposed in this work successfully predicts the observed rate behavior. Elementary step models have been developed. Comparison of the prediction of the models with the outcome of step change experiments leads to estimates of the rate constant for individual reaction steps. It has been shown that the rupture of the C–C bond in the surface C_2H_x species is likely to be the rate-limiting step under the conditions investigated. The results of model fitting at three temperatures for Ru/Al_2O_3 allow the activation energies of the proposed elementary steps to be determined. Ethane adsorption, accompanied by C–H bond breakage, has been shown to be an endothermic process.

1. INTRODUCTION

There is a growing interest in understanding the catalytic properties of ruthenium catalyst due to its high specific activity and good selectivity toward the production of higher hydrocarbons in the Fischer–Tropsch Synthesis (FTS) (*1–3*). Transient work on the FTS in this laboratory (*4, 5*) suggested that methylene groups formed from CO dissociation during the FTS play a significant part in the propagation process. It was suggested by McGenity (*4*) that the cracking of the C_{2+} hydrocarbons formed takes place simultaneously during the FTS in the presence of ruthenium catalysts. This is reasonable since ruthenium is an active hydrogenolysis catalyst (*6*). If we assume that the monocarbon fragments formed in ethane hydrogenolysis are the same as those encountered in the FTS, it is interesting to explore whether useful information on the FTS could be obtained by understanding the mechanism of ethane hydrogenolysis catalyzed by oxide-supported ruthenium catalysts.

Ethane hydrogenolysis has been studied by numerous authors (*6–21*). The majority of these studies have focused either on the mechanistic investigation of this reaction or on the evaluation of transition metal catalysts that catalyze the reaction. Although well studied, the mechanism of the reaction, largely derived from steady-state kinetic study, is still not clear. Moreover, there have been very few comprehensive investigations on the kinetics and mechanism of ethane hydrogenolysis over ruthenium catalysts.

The aim of the present work have been to study the kinetics of ethane hydrogenolysis on ruthenium catalyst at steady state and transient conditions over a wide range of feed compositions. Effort was made to discriminate between different kinetic models from the literature and those developed in this work. The transient technique was employed to obtain comparative and quantitative information on the rates of individual reaction steps, and thus on the mechanism of the reaction. It is suggested that transient experiments combined with

0021-9517/92 $3.00

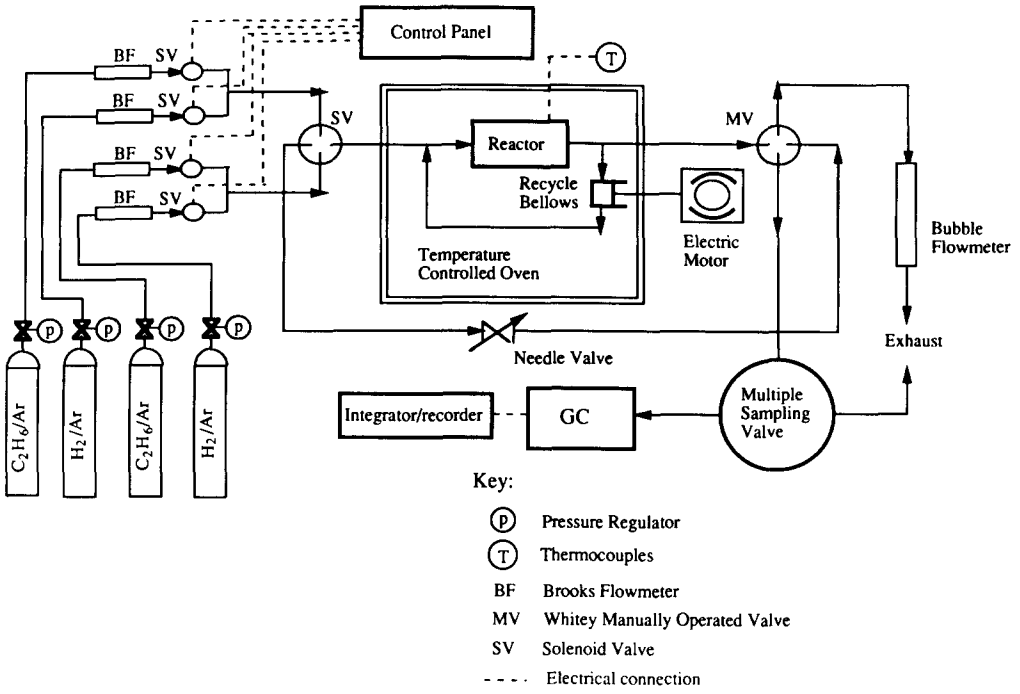

FIG. 1. Schematic diagram of the apparatus.

computer modeling is a powerful and promising method for obtaining insight into reaction mechanisms.

2. EXPERIMENTAL

Figure 1 shows a simple schematic description of the apparatus used in this work. The gases employed were supplied by Air Products Ltd. (all >99.5% pure) and were dried by passage over zeolite beads prior to entering the reactor. Flowrates were controlled using Brooks thermal mass flowmeters, which were interfaced to a PET microcomputer. This allowed flowrates to be set with an accuracy of ± 2% directly from the computer keyboard.

As Fig. 1 shows, two gas streams could be set up, each containing a mixture of H_2/Ar and C_2H_6/Ar of any desired composition. These were directed to a solenoid valve that has two inlet ports, one for each feed stream, and two outlet ports, one to a bypass line and the other to the reactor. The pressure in the bypass line was adjusted using a needle valve to ensure that the pressure in the two streams was equal. It has been shown that the switching of the solenoid valve gave a good approximation to a step change in feed composition (*4*).

The reactor used is an external recycle reactor. Recycling was achieved using a bellows pump. Step changes using He/Ar mixture showed that the reactor approximated very well to a CSTR (*5*).

A 16-port valve was employed for product sampling whereby seven samples could be captured. The capture of each sample takes only a few seconds and is afterward flushed into the GC. The analysis was carried out using a Pye 204 chromatograph with a flame ionization detector for hydrocarbons and a thermal conductivity detector for hydrogen. Chromatographic peaks were recorded and integrated by a Philips PU4811 integrator.

The catalyst used in this study is a commercially available Ru/Al_2O_3 supplied by Johnson Matthey Chemicals. The physical

TABLE 1

Physical Properties of the Catalyst

Catalyst	Ru/Al_2O_3
Metal loading (%)	0.48
Surface atom concentration (mol/g)[a]	3.69×10^{-5}
Surface area (m^2/g)[b]	1.8
Particle size (Å)	11
Dispersion (%)	74.6

[a] Determined by hydrogen temperature-programmed desorption.

[b] Calculated from the active site concentration by assuming equal participation of (100), (101), and (001) planes, and an average area of 8.7 $Å^2$/atom for ruthenium (*5*).

properties of the catalyst are shown in Table 1. The active surface area was determined using hydrogen temperature-programmed desorption.

All experiments were carried out at 1 atm pressure and a total flowrate of 100 cm^3/min except where the effect of total flowrate was examined. Steady-state experiments were performed to measure the effects of temperature, feed composition, and space velocity on the activity of the catalyst. Transient experiments consist of step changes between a feed of pure H_2 and a mixture of $H_2 : C_2H_6$.

To probe the kinetics of a catalytic reaction, it is necessary that heat and mass transfer resistances be very small. It has been shown by both experiment and calculation that under the experimental conditions chosen, both external and internal transport resistance are negligible (*5*).

3. MECHANISM AND KINETICS

Ethane hydrogenolysis catalyzed by Group VIII metals is generally explained using the following mechanism, which consists of three steps.

I. Adsorption Step

$$H_{2(g)} + 2S_v \rightleftharpoons 2H_{(s)}$$

$$C_2H_{6(g)} + 2S_v \rightleftharpoons C_2H_{5(s)} + H_{(s)}$$

$$C_2H_{5(s)} + H_{(s)} \rightleftharpoons C_2H_{x(s)} + aH_{2(g)} + S_v,$$

where S_v represents a vacant surface site, and x and a are integers related by $a = (6 - x)/2$.

Gudkov *et al.* (*18*) and Goddard *et al.* (*21*) have proposed a mechanism for ethane adsorption that consists of a series of steps to represent the formation of various surface hydrocarbon species. In practice, the rates of these vary according to the catalyst used and the reaction conditions employed. The above mechanism represents the overall behavior for the adsorption of hydrogen and ethane.

II. Fracture Step

$$C_2H_{x(s)} + \text{hydrogen} \rightarrow CH_{y(s)} + CH_{z(s)}.$$

III. Hydrogenation and Desorption Step

$$CH_{y(s)} + \text{hydrogen} \rightarrow CH_{4(g)}$$

$$CH_{z(s)} + \text{hydrogen} \rightarrow CH_{4(g)}.$$

This mechanism has been widely used in kinetic studies of ethane hydrogenolysis (*6*). In principle, any one of the three steps can be rate limiting. However, hydrogen adsorption at high temperature is expected to be much more rapid than any of the other steps. The processes of C–C bond rupture and of the hydrogenation of the methyl fragments have been reported to be the rate-limiting steps (*6–8, 17, 22*). The rate of ethane adsorption has also been assumed to be rate determining by Martin (*23*) while studying the kinetics of ethane hydrogenolysis over a nickel catalyst.

1. Steady-State Models

Due to the fact that there are no comprehensive modeling studies of ethane hydrogenolysis on ruthenium catalysts, a wide range of models, from the literature and also proposed in this work, have been used for steady-state modeling. Both the original model of Cimino *et al.* (*7*) and the modified form by Sinfelt and Taylor (*10*) ignored the surface covered by hydrogen. These models were extended in this work to account for the competition of hydrogen in ethane adsorption. The model proposed by Kristyan

and Szamosi (*19*) considered hydrogen adsorption together with multiple sites required for ethane adsorption. This model was also modified to account for the possibility that surface C_2H_x might occupy more than one site. Strictly speaking, the number of sites on the two sides of the reaction equation should balance. Thus, in some of the cases vacant sites are required to provide a site balance. Attempts were made in this respect for both the model proposed in this work and the model by Kristyan and Szamosi (*19*). Kristyan and Szamosi (*19, 20*) concluded from their study of ethane hydrogenolysis that the kinetically slow rupture of the C–C bond takes place in the presence of gaseous hydrogen. Our model was extended to consider the effect of splitting agents (i.e., vacant site, adsorbed hydrogen, or molecular hydrogen) on the rupture of the surface C–C bond. Formation of steady-state models was based upon assumptions of equilibrium adsorption of reactants and a rate-determining step. The derivation of model ES4 is presented here, for which the following reaction steps were assumed:

$$H_{2(g)} + 2S_v \overset{K_H}{\rightleftharpoons} 2H_{(s)}$$

$$C_2H_{6(g)} + S_v \overset{K_E}{\rightleftharpoons} C_2H_{x(s)} + aH_{2(g)}$$

$$C_2H_{x(s)} + H_{2(g)} \overset{k}{\longrightarrow} 2CH_{y(s)}$$

$$CH_{y(s)} + \text{hydrogen} \overset{\text{fast}}{\longrightarrow} CH_{4(g)}.$$

The application of the Langmuir equation for the adsorption of hydrogen and ethane gives

$$K_H P_H \theta_v^2 = \theta_H^2 \qquad (1)$$

$$K_E P_E \theta_v = \theta_x P_H^a, \qquad (2)$$

where K_H and K_E are the equilibrium adsorption constants of hydrogen and ethane, respectively, θ_H, θ_x, and θ_v are the surface coverage of H, C_2H_x, and vacant sites, and a is an integer. The surface coverage of $CH_{y(s)}$ is negligible since the hydrogenative desorption of this species was assumed to be fast. Thus, for competitive adsorption of hydrogen and ethane,

$$\theta_H + \theta_x + \theta_v = 1. \qquad (3)$$

Incorporating and solving Eqs. (1) to (3) give the expressions for the surface coverage of hydrogen and C_2H_x as,

$$\theta_H = \frac{(K_H P_H)^{0.5}}{1 + (K_H P_H)^{0.5} + (K_E P_E / P_H^a)} \qquad (4)$$

$$\theta_x = \frac{K_E P_E / P_H^a}{1 + (K_H P_H)^{0.5} + (K_E P_E / P_H^a)}. \qquad (5)$$

The rupture of the C–C bond in $C_2H_{x(s)}$ is assumed to be the rate-determining step in model ES4, and gaseous hydrogen is involved in this process. Thus, the reaction rate is given by

$$r = k\theta_x P_H = \frac{kK_E P_E P_H}{P_H^a (K_H P_H)^{0.5} + K_E P_E + P_H^a}. \qquad (6)$$

The same procedure applies to the derivation of other mechanistically based steady-state models. A summary of the steady-state models investigated is given in Table 2.

2. *Transient Model*

Both experimental observations and the results of steady-state modeling suggest that the adsorption of hydrogen and ethane is competitive. A simple elementary step model has been developed based on competitive adsorption. Assuming the reaction steps

$$H_{2(g)} + 2S_v \underset{k_2}{\overset{k_1}{\rightleftharpoons}} 2H_{(s)}$$

$$C_2H_{6(g)} + 2S_v \underset{k_4}{\overset{k_3}{\rightleftharpoons}} C_2H_{x(2s)} + aH_{2(g)}$$

$$C_2H_{x(2s)} + H_{2(g)} \overset{k_5}{\longrightarrow} 2CH_{y(s)}$$

$$CH_{y(s)} + (4 - y)H_{(s)} \overset{k_6}{\longrightarrow} CH_{4(g)} + (5 - y)S_v.$$

To formulate the equations for a model, consider the mass balance for a gas-phase component i.

TABLE 2

Summary of Steady State Models Studied

Model	Rate expression	Comments
ES1	$\text{Rate} = k P_E^{\alpha} P_H^{\beta}$	Power law rate
ES2	$\text{Rate} = \frac{kK_E P_E P_H}{K_E P_E + P_H^{a}}$	C_2H_6 adsorption equilibrium
ES3	$\text{Rate} = \frac{kP_E}{1 + bP_H^{a-1}}, \quad b = \frac{k_{-1}}{kK_2}$	C_2H_6 adsorption Nonequilibrium
ES4	$\text{Rate} = \frac{kK_E P_E P_H}{P_H^{a}(K_H P_H)^{0.5} + K_E P_E + P_H^{a}}$	Competitive H_2 adsorption
ES4A	$\text{Rate} = \frac{kK_E P_E P_H P_H^{a+1}}{[P_H^{a}(K_H P_H)^{0.5} + K_E P_E + P_H^{a}]^2}$	Vacant size required
ES4B	$\text{Rate} = \frac{kK_E P_E K_H^{0.5} P_H^{a+0.5}}{[P_H^{a}(K_H P_H)^{0.5} + K_E P_E + P_H^{a}]^2}$	Surface H required
ES5	$\text{Rate} = \frac{kK_E P_E P_H}{K_E P_E + (K_H P_H)(6 - x)/2 + (K_H P_H)(7 - x)/2]}$	Multiple sites H_2 competitive
ES5A	$\text{Rate} = \frac{kK_E P_E P_H (K_H P_H)(6 - x)/2}{[K_E P_E + (K_H P_H)(6 - x)/2 + (K_H P_H)(7 - x)/2]}$	Vacant site required
ES5B	$\text{Rate} = \frac{kK_E P_E (K_H P_H)(6 - x)/2}{[K_E P_E + (K_H P_H)6 - x/2 + (K_H P_H)7 - x/2]}$	Surface H required
ES5C	$\text{Rate} = k\theta_x P_H = k\{(B/2A)[B - (B^2 + 4A)^{0.5}] + 1\}P_H$	C_2H_x takes two sites
	$A = \frac{2K_E P_E}{(K_H P_H)(6 - x)/2}, \quad B = 1 + (K_H P_H)^{0.5}$	

$$V\frac{dC_i}{dt} = q^{\text{in}}C_i^{\text{in}} - qC_i + \sum_{j=1}^{l} m\nu_{ij}r_j, \quad (7)$$

where V is the reactor volume in m^3, C_i is the gas phase concentration of the i^{th} species in mol/m^3, q^{in} and q are the inlet and outlet flowrate, respectively, in m^3/s, m is the mass of the catalyst in g, r_j is the rate of reaction j in mol/g s, l is the number of reaction steps, and ν_{ij} is the stoichiometric coefficient for component i in the j^{th} reaction. It is often easier to deal with dimensionless quantities, so dividing both sides by (VC_T) leads to

$$\frac{dX_i}{dt} = \frac{1}{V}(q^{\text{in}}X_i^{\text{in}} - qX_i) + \frac{m}{VC_T}\sum_{j=1}^{l} \nu_{ij}r_j, \quad (8)$$

where C_T is the total gas-phase concentration in mol/m^3. While q^{in} remains constant, the outlet flowrate q may vary during an experiment and so it is convenient to eliminate q from the equations. To do this, sum over all components i

$$\sum_{i=1}^{n} X_i = \sum_{i=1}^{n} X_i^{\text{in}} = \alpha, \quad (9)$$

where α is a constant depending on the percentage of inert Ar present in the feed stream, and X_i^{in} and X_i are the mole fraction of i^{th} species in the feed and reactor outlet, respectively. Thus,

$$\sum_{i=1}^{n} \frac{dX_i}{dt} = 0 \quad (10)$$

$$\frac{q}{V} = \frac{q^{\text{in}}}{V} + \frac{m}{\alpha VC_T}\sum_{i=1}^{n}\sum_{j=1}^{l} \nu_{ij}r_j \quad (11)$$

let

$$\frac{m}{VC_T}\sum_{i=1}^{n}\sum_{j=1}^{l}\nu_{ij}r_j = \delta. \quad (12)$$

Therefore,

$$\frac{q}{V} = \frac{q^{in}}{V} + \frac{\delta}{\alpha}. \quad (13)$$

Substituting Eq. (13) into Eq. (8) gives

$$\frac{dX_i}{dt} = \frac{q^{in}}{V}(X_i^{in} - X_i) + \frac{m}{VC_T}\sum_{j=1}^{l}\nu_{ij}r_j - \frac{\delta}{\alpha}X_i. \quad (14)$$

Similarly, consider the mass balance for a surface species i

$$m\frac{dZ_i}{dt} = \frac{m}{S_T}\sum_{j=1}^{l}\nu_{ij}r_j, \quad (15)$$

where Z_i is the fractional coverage of i^{th} species, and S_T is the concentration of total active surface sites in mol/g.

It must be pointed out that given the level of complexity of the problem, allowance for the changes of rate constants with surface coverage is not considered here. There is growing evidence that the rate constants of elementary reaction steps do vary with changes in surface coverage due to heat of adsorption and reaction (*24*). However, these changes are unlikely to affect the conclusion of this work under the reaction conditions employed.

Most step changes consisted of switches from H_2/Ar to H_2/Ar and C_2H_6/Ar mixtures so that the initial conditions are clearly defined. The initial surface coverage can be estimated using the Langmuir equation since hydrogen is the only active species in the gas phase.

Having produced a model as a set of ordinary differential equations (ODEs) appropriate to the CSTR, initial estimates of the unknown parameters are made. The equations are then integrated numerically using the routine D02EBF from the library of the Numerical Algorithms Group, which employs Gear's method to integrate a set of

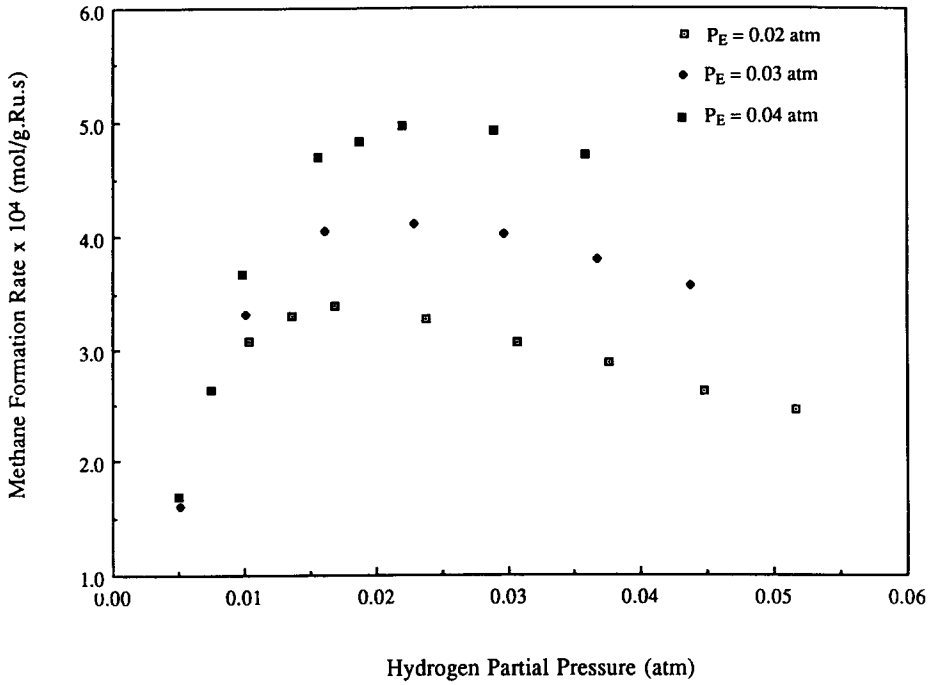

FIG. 2. Effect of hydrogen partial pressure on the rate of methane formation.

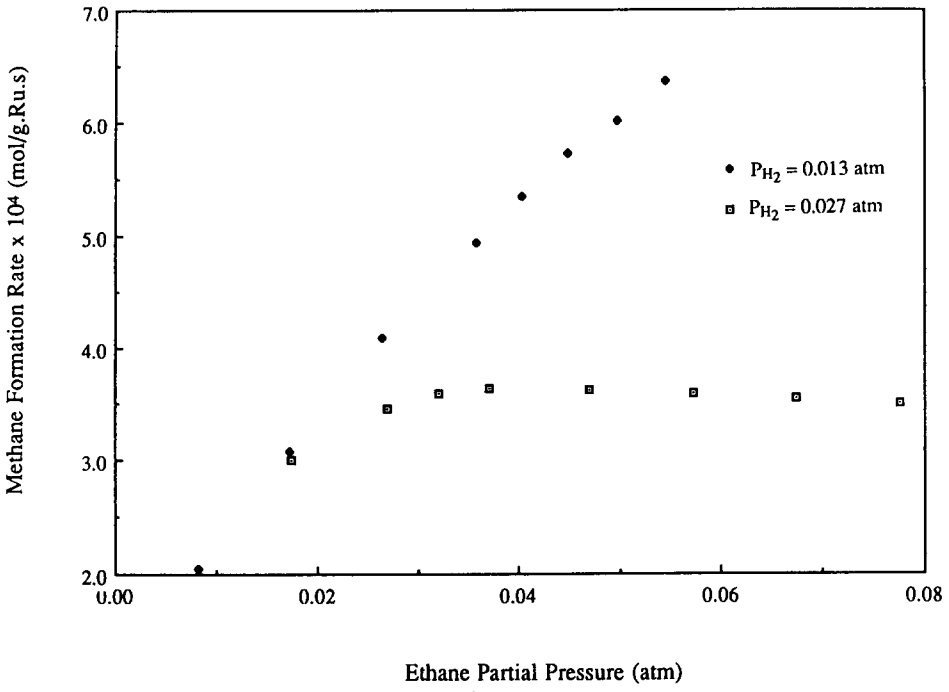

FIG. 3. Effect of ethane partial pressure on the rate of methane formation.

stiff, nonlinear ODEs. When the integration is completed, the optimization routine VA02AD, from the Harwell library, adjusts the values of the variable parameters, seeking to minimize the function

$$F(\mathbf{k}) = \sum_{t_i=0}^{t_0} (X^{t_i}_{\text{calc}} - X^{t_i}_{\text{expt}})^2, \qquad (16)$$

where $X^{t_i}_{\text{calc}}$ and $X^{t_i}_{\text{expt}}$ are the calculated and observed mole fractions, respectively, of methane at time t_i, $\mathbf{k}$ is the vector of variable parameters, and the summation is over all the points in time at which experimental measurements were made, up to and including the last point (at t_0). The program stops when $F(\mathbf{k})$ has reached a minimum (i.e., the best fit of the model to the experimental data).

4. RESULTS

1. Steady-State Results

Experiments showed that the catalyst deactivated in all feed conditions, but the extent varies with feed $H_2 : C_2H_6$ ratio. Deactivation is more significant at the initial stage of the reaction. A time on stream of 15 min was used prior to the measurement of the steady-state rate. The catalyst was reduced in hydrogen after each experiment to clean any surface CH_x species present.

The rates of methane formation determined over a temperature range of 158–223°C fitted well to the Arrhenius plot, which gave an activation energy of 102.7 kJ/mol for a feed $H_2 : C_2H_6$ ratio of 1 : 1. This is in agreement with the published literature values for ruthenium catalysts (*25*).

Figures 2 and 3 show the effects of hydrogen and ethane partial pressure on the rate of methane formation. Figure 2 shows clearly that over a wide range of feed compositions, the effects of hydrogen partial pressure on the reaction rate can be divided into two parts. Once the partial pressure of hydrogen is small, the rate increases with increasing hydrogen partial pressure and reaches a maximum. When the partial pressure of hy-

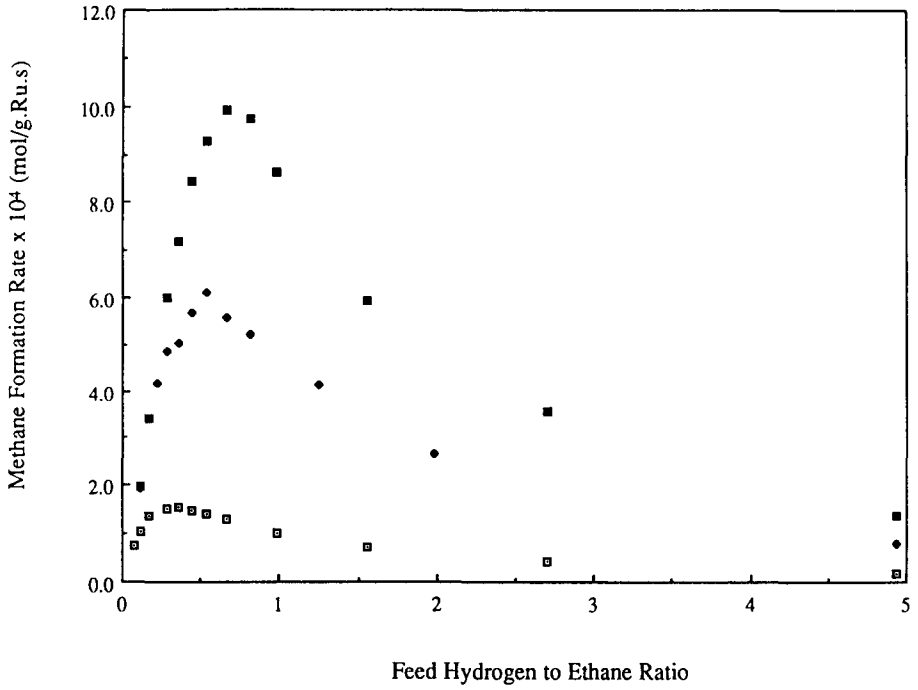

FIG. 4. Effect of temperature on the dependence of methane formation rate on hydrogen to ethane ratio. (□) T = 180°C; (◆) T = 200°C; (■) T = 220°C.

drogen exceeds a certain value, any further increase in hydrogen partial pressure suppresses the reaction rate. With ethane, the rate is proportional to its partial pressure, but only up to a limit, beyond which it is almost independent of ethane partial pressure.

Figure 4 shows the effect of hydrogen to ethane ratio on the reaction rate at three different temperatures. The pressures of both hydrogen and ethane were altered simultaneously in this case. The hydrogen to ethane ratio corresponding to the rate maximum shifts to a higher value as the temperature is increased. This is consistent with the finding of Sinfelt and Taylor (*10*) over a silica-supported cobalt catalyst.

Figure 5 shows some of the results of steady-state model fitting to the experimental data. The modified forms of models ES4 and ES5 showed little difference from the original models; the results from these models are therefore not presented here. Table 3 gives detailed results from model fitting. Included in this table are the number of hydrogen molecules released during ethane adsorption (for models ES2, ES3, and ES4) or the number of hydrogen atoms remaining in the surface C_2H_x species (for model ES5). This parameter was fixed during modeling and its value was altered by repeating the modeling process. The values given in Table 3 are those that produce the best fit for each of the models. A power law rate equation fails to fit the kinetic data over the whole range of partial pressures as simple exponents cannot account for the observed rates that display a maximum. For completeness, model fitting to power law equations was accomplished correlating the data over two ranges, i.e., hydrogen rich and ethane rich. The results are summarized in Table 3 (model ES1) with the exponents lying in acceptable ranges.

To visualize the rate surface, model prediction using the parameters found by fitting

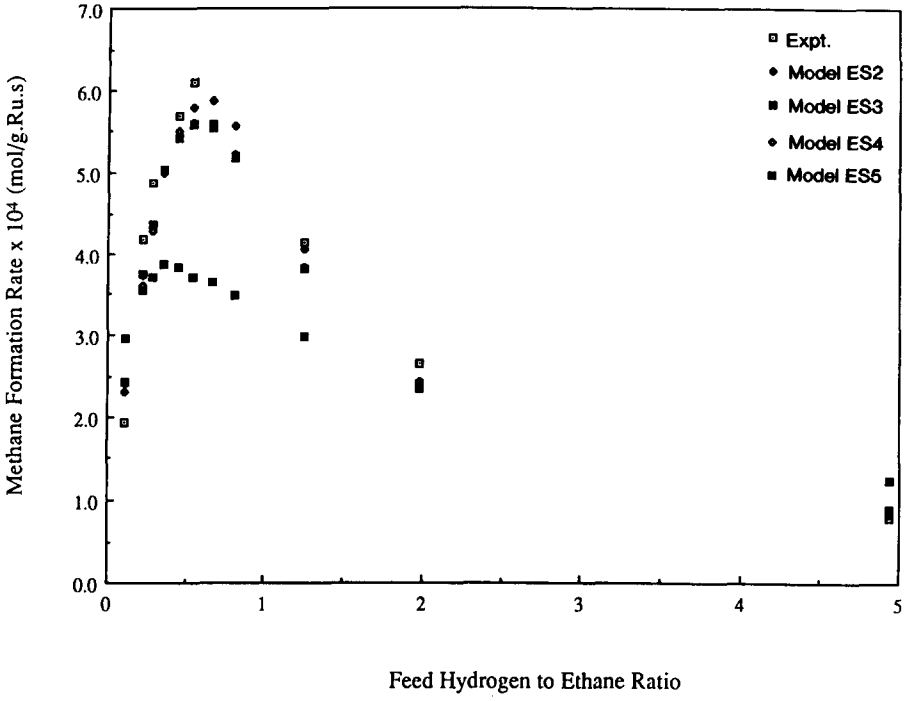

FIG. 5. Steady-state model fittings.

model ES4 was carried out for a temperature of 200°C, as shown in Fig. 6. As can be seen, the predicted rate surface over the whole range of feed compositions reflects the experimentally observed effects of hydrogen and ethane partial pressure on the rate of methane formation. The response surface is consistent with competitive adsorption of ethane and hydrogen.

2. *Transient Results*

As with the steady-state models, the transient model also has an adjustable parameter, a (the number of hydrogen molecules released during ethane adsorption), which determines the composition of the adsorbed surface hydrocarbon species. However, unlike the steady-state model fitting, it was found to be easier to discriminate between different values of a although this involved a great deal of tedious computation. $a = 1$ was found to give best fits to step changes from hydrogen to 1 : 1 $H_2 : C_2H_6$ at three different temperatures and flowrates.

Figure 7 shows the result of fitting the transient model described previously to step changes from hydrogen to 1 : 1 $H_2 : C_2H_6$ at 200°C and a total flowrate of 100 cm^3/min. The parameter values derived from the model fitting are summarized in Table 4. The units of these constants are all normalized to reciprocal seconds since it is desirable to have a standard convention to be able to compare the results obtained in our research group at various stages. The normalization was carried out by utilizing constant values representing the properties of the reaction system, i.e., total gaseous concentration and concentration of catalytic sites.

The normalization of the rate constant for hydrogen adsorption is given here as an example. The rate of hydrogen adsorption in the transient model was defined as

$$r_a = k_1 C_H S_v^2, \tag{17}$$

where r_a is the rate of hydrogen adsorption in mol/gs, C_H is the concentration of gaseous hydrogen in mol/m^3, and S_v is the con-

TABLE 3

Results of Steady-State Model Fitting

Model		Parameters			RMS %
		α	β		
ES1					
	H_2 rich	0.6	0.9		16.5
	C_2H_6 rich	0.0	−0.4		18.4
ES2	a	k (mol/g s atm)	K_E		
	3	1.44×10^{-4}	1.06×10^{-3}		10.4
ES3	a	k_1 (mol/g s atm)	b		
	0	8.16×10^{-5}	3.24×10^{-2}		34.5
ES4	a	k (mol/g s atm)	K_E	K_H (atm^{-1})	
	2	1.52×10^{-4}	1.45×10^{1}	1.10×10^{7}	9.0
ES5	x	k (mol/g s atm)	K_E	K_H (atm^{-1})	
	2	1.53×10^{-4}	2.08×10^{7}	7.31×10^{3}	14.3

centration of surface vacant sites in mol/g. The units for the rate constant of hydrogen adsorption is then given as

$$[k_1] = \frac{[\text{gm}^3]}{[\text{mol}^2\text{s}]}.$$

Multiplying the above expression by $(C_T S_T)$, which are the total gaseous concentration and concentration of catalytic sites, respectively, leads to

$$[k_1'] = \frac{[\text{gm}^3]}{[\text{mol}^2\text{s}]}\frac{[\text{mol}]}{[\text{m}^3]}\frac{[\text{mol}]}{[\text{g}]} = [\text{s}^{-1}].$$

A similar procedure applies for the rate constants of other reaction steps.

To examine the range of validity of the model, the values so derived were used to predict the transient behavior in other experiments. Figures 8 to 12 show examples of such predictions. As shown in Fig. 9, step changes from hydrogen to 1/13 $H_2 : C_2H_6$ provide a demanding test of both the validity and the limitation of the simple transient model.

Figures 13 and 14 show the results of fitting the model to step changes from hydrogen to 1 : 1 $H_2 : C_2H_6$ at 176 and 221°C and flowrates of 80 and 90 cm^3/min, respectively. Table 4 summarizes the parameter values obtained.

The results of fitting the transient model at three temperatures are well represented by an Arrhenius-type rate dependence on temperature for the proposed individual reaction steps. The activation energies obtained are presented in Table 5.

The predicted surface coverages of various species for two feed compositions are shown in Table 6. These predictions were made for a time on stream of 200 s. It is shown clearly that adsorbed hydrogen is the dominant surface species for a stoichiometric feed mixture. This is true for most of the feed conditions. The adsorbed C_2H_4 becomes the major surface species only for feed mixtures extremely rich in ethane. Moreover, the coverage of the surface by monocarbon species is negligibly low for all feed conditions.

5. DISCUSSION

The rate of methane formation for ethane hydrogenolysis has been measured over a wide range of feed compositions on

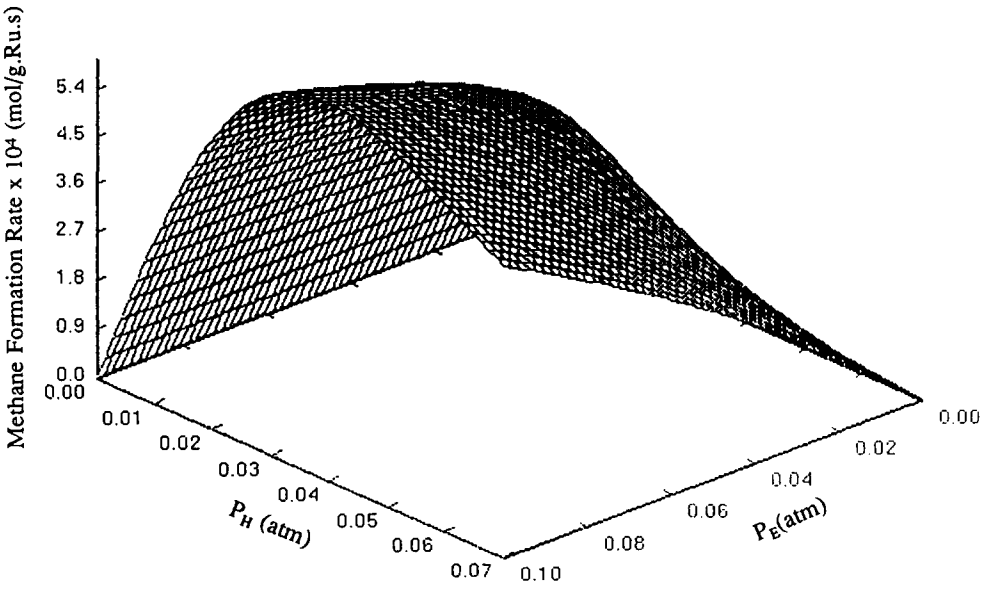

FIG. 6. Prediction of methane formation rate surface using model ES4. Temperature, 200°C. Flowrate, 100 cm³/min. Rate = $kK_EP_EP_H/(P_H^a(K_HP_H)^{0.5} + K_EP_E + P_H^a)$, where $a = 2$, $K_E = 14.5$, $K_H = 1.10 \times 10^7$, $k = 1.52 \times 10^{-4}$.

Ru/Al_2O_3 catalyst. The general behavior of the ruthenium catalyst is similar to that of other Group VIII metals. It has been shown that the rate of methane formation is a function of both the partial pressures of ethane and hydrogen. A positive order dependence of the rate on ethane partial pressure is observed within a limit, beyond which the rate is independent of ethane pressure. The dependence of rate on hydrogen pressure goes through a maximum, the effect of which varies with temperature. Gudkov *et al.* (*18*) made a similar observation in their study of ethane hydrogenolysis over a Pt catalyst. This phenomenon strongly suggests that hydrogen is competing for surface sites with ethane upon adsorption.

A range of steady-state models has been tested. It is concluded that a simple steady-state model (ES4) based on competitive adsorption of hydrogen and ethane can successfully explain the experimental observations. As shown in Fig. 6, the surface coverage by hydrogen must be higher than that by hydrocarbon species for most of the feed compositions since it takes a much higher ethane partial pressure to cause a decrease in the rate. It seems that hydrogen is more easily adsorbed than ethane on the ruthenium surface during ethane hydrogenolysis. This is consistent with the transient prediction of surface coverages by different adsorbed species. For a feed mixture of 1 : 1 $H_2 : C_2H_6$ the transient model predicted that adsorbed hydrogen is the major surface species (see Table 6).

Comparison of rate constants for various individual steps obtained from transient

TABLE 4

Parameter Values from Transient Model Fitting

Temperature (°C): Parameters (s^{-1})	176	200	221
k_1'	1.20×10^6	1.68×10^6	2.44×10^6
k_2'	2.30×10^5	3.24×10^5	9.51×10^5
k_3'	7.56×10^8	2.50×10^9	6.21×10^9
k_4'	1.04×10^{10}	1.81×10^{10}	5.25×10^{10}
k_5'	1.57×10^1	2.48×10^1	7.25×10^1
k_6'	1.07×10^7	1.09×10^8	1.09×10^8

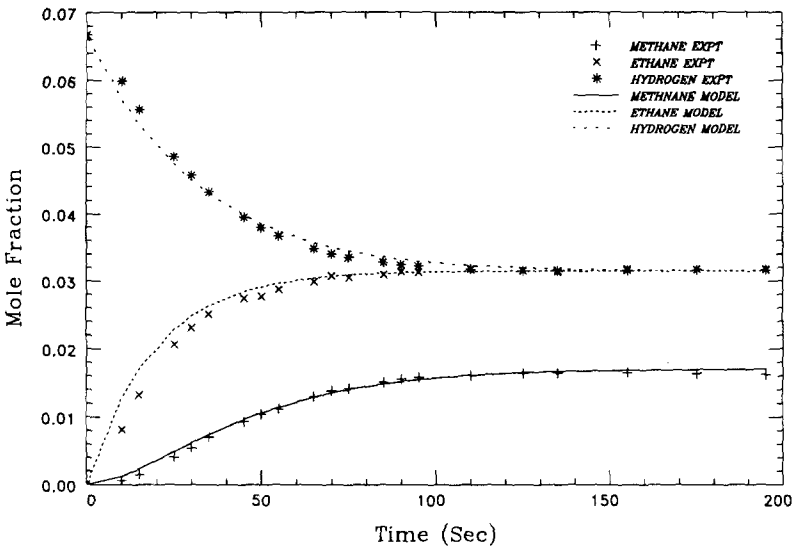

FIG. 7. Transient model fitting for step change of $H_2 \rightarrow$ 1:1 H_2:C_2H_6. Temperature, 200°C. Flowrate, 100 cm^3/min.

modeling reveals that the breaking of the C–C bond in the adsorbed C_2H_x is the slow step. This provides confirmation of the conclusions of the majority of the published steady-state kinetic studies on ethane hydrogenolysis (*26*). The hydrogenative desorption of surface monocarbon species is fast and confirms the general view that this step is kinetically insignificant (*6, 21*).

The results presented for the transient studies show clearly that the rate constants derived from transient model fitting at differ-

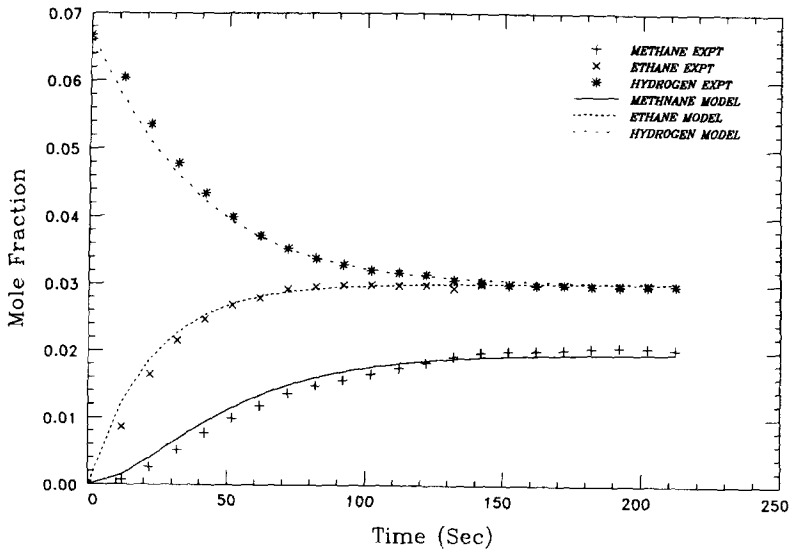

FIG. 8. Transit model prediction for step change of $H_2 \rightarrow$ 1:1 H_2:C_2H_6. Temperature, 200°C. Flowrate, 80 cm^3/min.

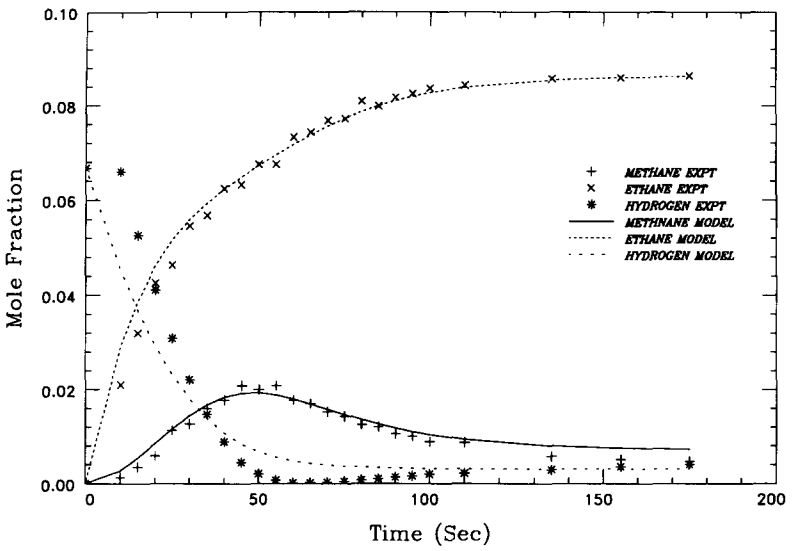

FIG. 9. Transient model prediction for step change of $H_2 \rightarrow$ 1:13 H_2:C_2H_6. Temperature, 200°C. Flowrate, 100 cm^3/min.

ent temperatures display an Arrhenius-type temperature dependence. The enthalpy derived from this temperature dependence of the rate of ethane adsorption, indicates that this process, accompanied by the rupture of C–H bonds, is an overall endothermic process. However, the same consistency cannot be achieved for the parameter values from steady-state modeling. Indeed, multiple solutions were encountered during steady-state modeling in terms of K_H and K_E. This shows the advantage of transient

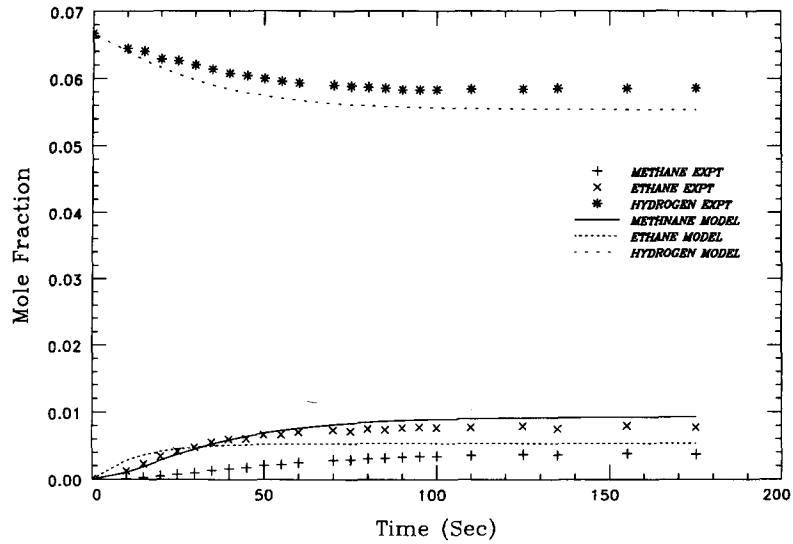

FIG. 10. Transient model prediction for step change of $H_2 \rightarrow$ 13:1 H_2:C_2H_6. Temperature, 200°C. Flowrate, 100 cm^3/min.

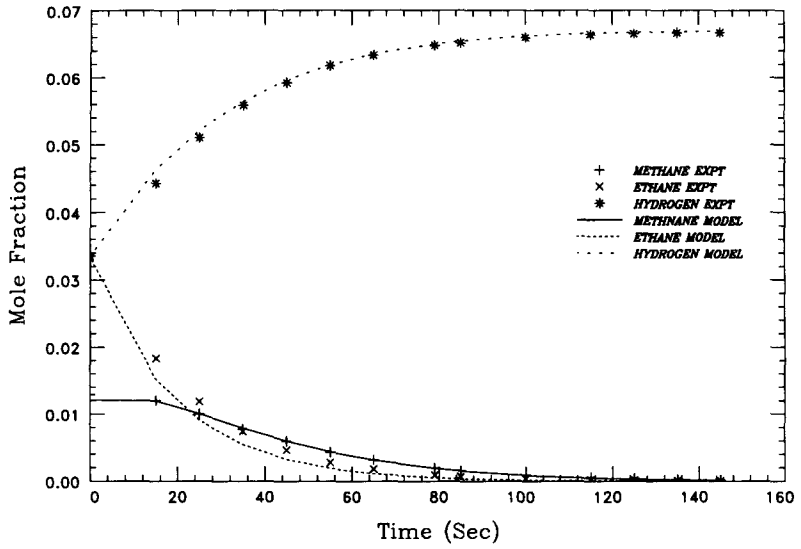

FIG. 11. Transient model prediction for step change of 1:1 H_2:C_2H_6 → H_2. Temperature, 200°C. Flowrate, 100 cm^3/min.

modeling as discussed by Kobayashi and Kobayashi (*27*) and Bennett (*28*).

Both the steady-state models and the transient model studied have an adjustable parameter a or x ($a = (6 - x)/2$), which determines the composition of the adsorbed surface C_2H_x and CH_y species. It was found difficult to discriminate between different values of a in the steady-state models. However, it was easier in the case of transient

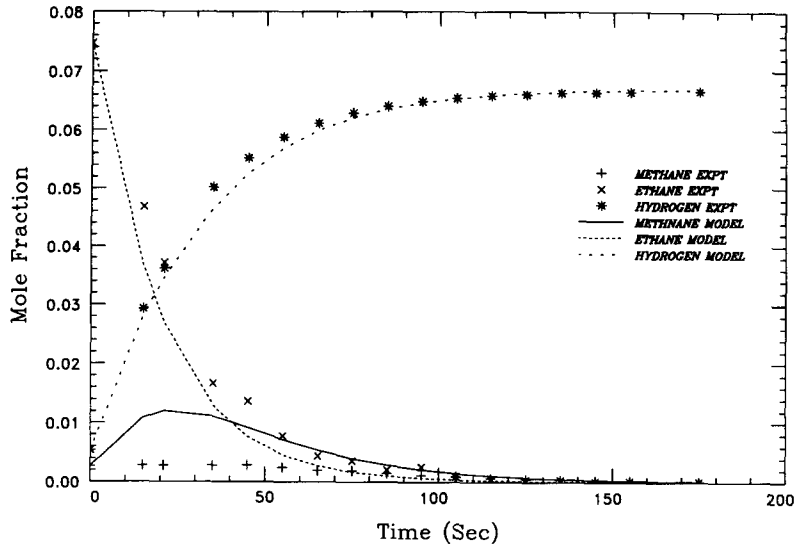

FIG. 12. Transient model prediction for step change of 13:1 H_2:C_2H_6 → H_2. Temperature, 200°C. Flowrate, 100 cm^3/min.

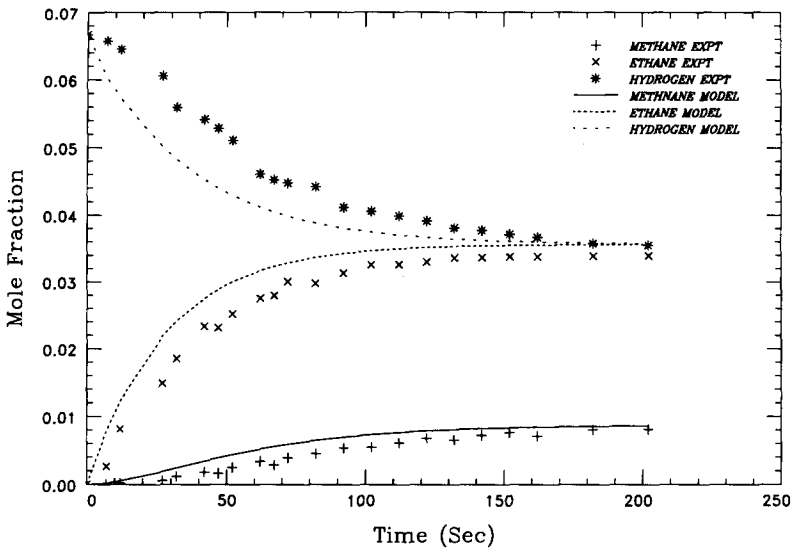

FIG. 13. Transient model fitting for step change of $H_2 \rightarrow$ 1:1 H_2:C_2H_6. Temperature, 176°C. Flowrate, 80 cm^3/min.

modeling although this involved a great deal of tedious computation. Consequently, the parameter values derived from steady-state modeling can vary over a wide range, and it is difficult to draw quantitative comparison between the results from steady-state and transient modeling. On the other hand, the results from transient modeling do justify some of the assumptions made in the steady-state models, as explained in the following.

Using the reaction scheme for the transient model, the steady-state description of

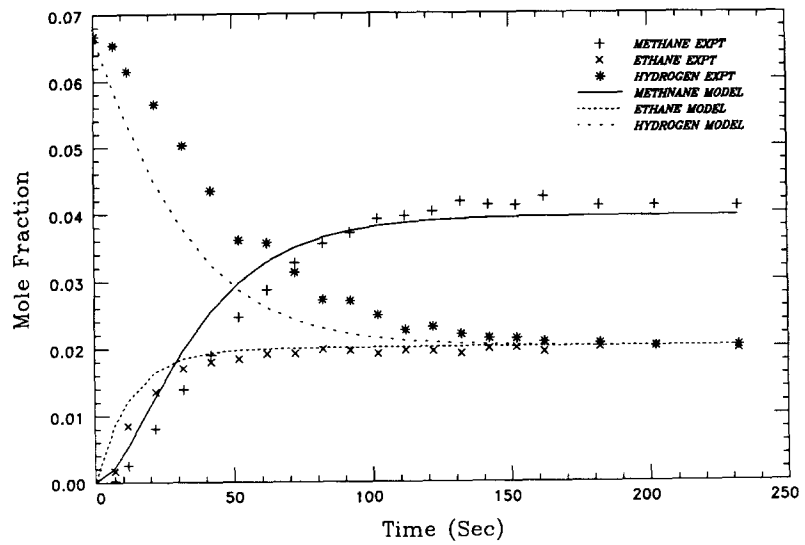

FIG. 14. Transient model fitting for step change of $H_2 \rightarrow$ 1:1H_2:C_2H_6. Temperature, 221°C. Flowrate, 90 cm^3/min.

TABLE 5

Temperature Dependence of Selected Rate Constants

Step	Activation energy (kJ/mol)
H_2 adsorption	33.0
H_2 desorption	57.9
C_2H_6 adsorption	89.0
C_2H_x desorption	69.2
C–C rupture	66.6

the system, following Petersen (*29*), is given by

$$S_1 + 2S_2 + S_3 + S_v = S_T$$

$$dS_1/dt = 2k_1C_1S_v^2 - 2k_2S_1^2 - k_6S_3S_1^{4-y} = 0$$

$$dS_2/dt = k_3C_2S_v^2 - k_4S_2C_1^a - k_5S_2C_1 = 0$$

$$\frac{dS_3}{dt} = 2k_5C_1S_2 - k_6S_3S_1^{4-y} = 0,$$

where S_1, S_2, S_3, and S_v are the concentrations of surface H, C_2H_x, CH_y, and vacant sites, respectively, in mol/g, and C_1 and C_2 are the concentrations of gaseous hydrogen and ethane in mol/m^3.

Rearranging the above set of equations with $a = 1$ and $y = 3$, which produced the best fits for the catalyst studied, gives

$$S_1 = \frac{1}{k_2^{0.5}}\left(k_1C_1 - \frac{k_3k_5C_2}{k_4 + k_5}\right)^{0.5} S_v$$

$$S_2 = \frac{k_3C_2}{(k_4 + k_5)\,C_1} S_v^2$$

$$S_3 = \frac{2k_2^{0.5}k_3k_5C_2}{k_6(k_4 + k_5)\,[k_1C_1 - k_3k_5C_2/(k_4 + k_5)]^{0.5}} S_v.$$

TABLE 6

Predicted Surface Coverages for Feed of 1:1 H_2:C_2H_6 and of 1:13 H_2:C_2H_6 at t = 200 s after Switch

Feed composition	$H_{(s)}$	$C_2H_{4(s)}$	$CH_{3(s)}$
1:1	0.26	0.057	3.3×10^{-9}
1:13	0.032	0.35	1.3×10^{-8}

Note. Temperature, 200°C. Flowrate, 100 cm^3/min.

Now, consider the set of rate constants obtained from fitting the transient model to step changes from hydrogen to 1:1 $H_2:C_2H_6$ at 200°C (Fig. 7).

$$k_1 = 1.50 \times 10^9 \text{ m}^3\text{g/mol}^2 \text{ s}, \qquad k_2 = 9.44 \times 10^9 \text{ g/mol s}$$

$$k_3 = 1.36 \times 10^{12} \text{ m}^3\text{g/mol}^2 \text{ s}, \qquad k_4 = 7.09 \times 10^8 \text{ m}^3\text{/mol s}$$

$$k_5 = 1.35 \times 10^0 \text{ m}^3\text{/mol s}, \qquad k_6 = 1.97 \times 10^{12} \text{ g/mol s}.$$

Since $k_4 \gg k_5$, and $C_1 = C_2$ at steady state in this example, then,

$$k_1C_1 \gg \frac{k_3k_5}{k_4} C_2.$$

The above expressions for the concentrations of $H_{(s)}$ and $C_2H_{4(s)}$ can then be simplified as

$$S_1 = \left(\frac{k_1}{k_2}C_1\right)^{0.5} S_v, \quad S_2 = \left(\frac{k_3C_2}{k_4C_1}\right) S_v^2.$$

The corresponding surface coverages of the two species are

$$\theta_1 = \left(\frac{k_1}{k_2}C_1\right)^{0.5} \theta_v, \quad \theta_2 = \left[\frac{(k_3S_T)\,C_2}{k_4C_1}\right] \theta_v.$$

These are the same as those expected from the Langmuir expression. Noting that the rate of the forward step for ethane adsorption is proportional to the square of the concentration of vacant surface sites, while the rate of the reverse step is proportional to the concentration of $C_2H_{4(s)}$ only, (k_3S_T) can be regarded as the modified rate constant for the forward step. Therefore, the assumptions made in steady-state model ES4, of equilibrium adsorption of hydrogen and ethane, and of C–C bond rupture being the rate-limiting step are justified.

Given the complexity of the processes occurring on the catalyst surface and the neglect of factors such as different kinds of adsorption sites, surface coverage dependent heat of adsorption and adsorbate mobility, the ability of the proposed transient model to provide a quantitative description

of the transient process over a wide range of feed compositions represents an improvement to the current understanding of ethane hydrogenolysis on a ruthenium catalyst.

ACKNOWLEDGMENTS

The authors acknowledge the Chancellor's Fund, Cambridge University, for financial support. The useful discussion with Professor C. O. Bennett is gratefully acknowledged.

REFERENCES

1. King, D. C., *J. Catal.* **51,** 386 (1978).
2. Smith, K. J., and Everson, R. C., *J. Catal.* **99,** 349 (1986).
3. Zhou, X., and Gulari, E., *J. Catal.* **105,** 499 (1987).
4. McGenity, P. M., Ph.D. thesis, University of Cambridge, 1987.
5. Shang, S. B., Ph.D. thesis, University of Cambridge, 1989.
6. Sinfelt, J. H., *Catal. Rev.-Sci. Eng.* **3(2),** 175 (1969).
7. Cimino, A., Boudart, M., and Taylor, H. S., *J. Am. Chem. Soc.* **58,** 96 (1954).
8. Anderson, J. R., and Baker, B. G., *Proc. R. Soc. Ser. A* **271,** 402 (1963).
9. Sinfelt, J. H., and Yates, D. J. C., *J. Catal.* **8,** 82 (1967).
10. Sinfelt, J. H., and Taylor, W. F., *Trans. Faraday Soc.* **64(4),** 3086 (1968).
11. Sinfelt, J. H., and Yates, D. J. C., *J. Catal.* **10,** 362 (1968).
12. Sinfelt, J. H., *in* "Advances in Catalysis" (D. D. Eley, H. Pines, and P. B. Weisz, Eds.), Vol. 23, P. 91. Academic Press, New York, 1973.
13. Guczi, L., Gudkov, B. S., and Tétényi, P., *J. Catal.* **24,** 187 (1972).
14. Frennet, A., Degols, L., Liénard, G., and Crucq, A., *J. Catal.* **35,** 18 (1974).
15. Sárkány, A., Matusek, K., and Tétényi, P., *J. Chem. Soc. Faraday Trans. 1* **73,** 1699 (1977).
16. Tétényi, P., Guczi, L., and Sárkány, A., *Acta Chim. Acad. Sci. Hungar.* **97,** 221 (1978).
17. Foster, H., and Ötto, J., *Z. Phys. Chem. N.F.* **120,** 223 (1980).
18. Gudkov, B. S., Guczi, L., and Tétényi, P., *J. Catal.* **74,** 207 (1982).
19. Kristyan, S., and Szamosi, J., *J. Chem. Soc. Faraday Trans. 1* **80,** 1645 (1984).
20. Kristyan, S., and Szamosi, J., *J. Chem. Soc. Faraday Trans. 1* **84,** 91 (1988).
21. Goddard, S. A., Amiridis, M. D., Reoske, J. E., Cardona-Martinez, N., and Dumesic, J. A., *J. Catal.* **117,** 155 (1989).
22. Sinfelt, J. H., *J. Catal.* **27,** 468 (1972).
23. Martin, G. A., *J. Catal.* **60,** 345 (1979).
24. Boudart, M., and Djega-Mariadassou, G., "Kinetics of Heterogeneous Catalytic Reactions." Princeton Univ. Press, Princeton, NJ, 1984.
25. Galvagno, S., Schwank, J., Gubitosa, G., and Tauszik, G. R., *J. Chem. Soc. Faraday Trans. 1* **78,** 2509 (1982).
26. Guczi, L., Frennet, A., and Ponec, V., *Acta Chim. Acad. Sci. Hungar.* **112(2),** 127 (1983).
27. Kobayashi, H., and Kobayashi, M., *Catal. Rev.-Sci. Eng.* **10,** 139 (1974).
28. Bennett, C. O., *Catal. Rev.-Sci. Eng.* **13,** 121 (1976).
29. Petersen, E. E., "Chemical Reaction Analysis." Prentice–Hall, Englewood Cliffs, NJ, 1965.